From patterning heterogeneity to nanoglass: A new approach to harden and toughen metallic glasses

Yongwei Wang, Herbert Gleiter, and Mo Li*

Monolithic metallic glass is a quasi-brittle material with little plasticity on a continuum scale, but tremendous local plasticity in nano- and micron scales. One way to enhance the macroscopic plasticity and toughness is to make composites with inclusions that can alter the local shear behavior. By far, however, the attempt still faces tremendous challenges. Here, we propose a new concept by introducing microstructures into the structureless glasses by spatially patterning the heterogeneities. One case study shown here is to form the stochastically distributed glass domains or "grains" and their boundaries that have different kinds of heterogeneities. We demonstrate that the granular metallic glass (GMG) can be toughened and even "hardened" by tuning the grain-boundary width, amount of free volumes, and grain size. The hardening mechanisms in the emerging GMG are intricately related to how shear banding is blocked or promoted by the spatially patterned heterogeneity if proper length scales of the heterogeneities are organized and function synchronously.

Impact statement

Different from crystalline materials, glassy materials do not have ordered atomic structures. As a result, they all appear brittle macroscopically, which includes metallic glasses despite the well-known metallic bond-ing that supposedly gives rise to ductility. As a twist, different from other types of glasses such as oxide glasses, metallic glasses possess tremendous ductility in nanometer and micrometer scales. Therefore, how to manage the microscopic ductility and extend it to macroscopic scale becomes one of the most challeng-ing engineering as well as scientific problems facing materials scientists and engineers.

In this article, we present a "thought-experiment" to predict the possibility and viability of enhancing the plasticity of metallic glasses, and its strength as well. The main idea is to create a new design of the glassy materials, the granular glass, via spatially patterning heterogeneities. To prove this idea, we used finite element modeling. The extensive work and analysis show that this new approach is not only possible but effective in "engineering" ductility in the materials that are known as "brittle." We expect this work to stimulate experiments that can turn this idea into reality.

Introduction

Metallic glasses (MGs) inherit many superb mechanical properties known for crystalline metals, such as high strength and large ductility. However, the ductility is largely limited in nano and micron scales via the so-called shear localization.[1–4] Shear banding renders the MGs brittle macroscopically because the deformation in the shear banding regions can become so localized and so large that the samples lose their load-bearing ability there at yielding and fracture abruptly as a result. Therefore, how to manage the large microscopic deformation and enhance the macroscopic ductility becomes a major open problem in scientific research and industrial development for the past decade.[1,3–7]

The first natural choice is either mixing or precipitating out some hard phases in MG forming liquids to obtain the composites with extensive plasticity that is otherwise absent in monolithic MGs.[1,3–14] The hard inclusions in the MG matrix can change the local shear behavior by either blocking the propagating shear bands, altering their paths, or initiating new shear bands. For optimal outcome, a certain amount of hard phases need to be distributed uniformly with proper separation distances between them such that the local shear bands can be effectively blocked or altered. However, it is technically challenging to mix uniformly the solid particles or fibers with nano or micron sizes in the viscous MG melts that have a narrow window of operating temperature and time before they turn into solid.[7–10] Often, the inclusions become clumped or aggregated, which make the composites less effective, or even more

Yongwei Wang, Collaborative Innovation Center of Steel Technology, University of Science and Technology Beijing, Beijing, China
Herbert Gleiter, Institute of Nanotechnology, Karlsruhe Institute of Technology, Karlsruhe, Germany
Mo Li, School of Materials Science and Engineering, Georgia Institute of Technology, Atlanta, USA; mo.li@gatech.edu
*Corresponding author

susceptive to abrupt fracture caused by local stress concentration in these areas. An alternative is by precipitating hard crystalline phases from the melt during cooling, such that a ductile MG composite can be obtained that has finely dispersed inclusions such as tungsten dendrites.[11–14] Obviously, this method is applicable only for certain metals with high melting point so they can crystallize in the MG forming liquids during cooling.

To maximize the effects, a large amount of inclusions need to be introduced in practice. Sometimes more than 60% volume fraction or more of particles, fibers or precipitated crystal dendrites were used.[8–10] This, ironically, makes the MG a minority phase in the composites. In addition, some inclusions are costly and technically cumbersome in processing. As a result, making MG composites with easy processing and better performance remains a challenge. The universal underlying issue is the incompatibility in the strength or strain limit between the inclusions and MG matrix that causes stress concentration and eventual interface debonding and internal cracking.

To overcome these limitations, different strategies are devised. Rather than using the (crystalline) phases that have the sharp change at the interfaces, which cause the incompatibility, "inclusions" made of various heterogeneities are introduced, which still maintain the amorphous structure, but with gradual change in mechanical properties across the interface. For example, by chemical segregation, finely dispersed inclusions in the form of chemical concentration variations can be obtained.[15–17] Our early theoretical work reveals that indeed, these chemical heterogeneities have different densities or free volumes (FVs) that can greatly improve macroscopic ductility, and at the same time, even enhance the strength if proper choice of statistical distributions for the FVs could be managed.[18–21] In addition, we found that the spatial distribution of these FVs can also play a significant role. Because the local shear deformation occurs in the directions around the maximum resolved shear stress (MRSS), the spatial distribution, or how the patterns of the heterogeneous FV regions are oriented, is critical to the formation and propagation of shear bands.[20] For example, if the different FV regions are stripes as in the chemical spinodal decomposed MGs, when they are aligned in the direction within the proximity of the MRSS, the orientation of these stripe regions can become effective in initiating shear bands and promote shear propagation as well.[20] If the orientation is made perpendicular to the direction of the MRSS, the tendency can be greatly reduced, thus, enhancing the strength. Therefore, by simply changing the shape and orientation of the heterogeneities, one can effectively improve the plasticity as well as strength of the MGs.

The chemical segregation or precipitation of new phases is a natural process where the orientations and shapes of the heterogeneous regions are not often optimized automatically as desired. In addition, there are other factors that we can exploit in patterning heterogeneities but are not accustomed to think about for MGs. These include the size of the domains, the interfaces between two adjacent MG domains, and the FV densities in different regions. These factors are widely known and used in engineering polycrystals, but little in MGs because of the lack of any structure *per se*. The challenges in making MG composites and taking the potential advantages in patterning heterogeneities motivate us to think of a new strategy by artificially patterning the heterogeneities in desired shape and size, as well as orientation to improve the plasticity in MGs.

In analogy to polycrystals, we introduce "microstructures" into the structureless glassy materials. The polycrystal-like microstructure is also called stochastic pattern, which consists of grains and boundaries. It can be made in experiment either through synthesis or by 3D printing. Inert gas condensation (IGC) or vapor deposition (VD) have been used to form MG particles that are assembled randomly into "polycrystal," or granular patterns such as in synthesis of nanocrystal and nanoglass (NG).[22–26] The traditional sintering methods in powder metallurgy can also produce the pattern. Besides this simple stochastic microstructure, there are many other microstructure patterns. In **Figure 1**, we show some of these patterns. Despite the difference, they all consist of domains of heterogeneities and the boundaries between the domains. The differently colored domains, for example, represent regions of different FV densities used as a convenient parameter to represent heterogeneity in MGs. Except in Figure 1a, which is a traditional composite with isolated particles or fibers mixed in the continuous MG matrix, the others have connected domains, including the spinodal decomposed bicontinuous MG regions (Figure 1b), honeycomb lattice (Figure 1c), as well as polycrystalline or Voronoi microstructure previously discussed (Figure 1d). Each domain has a certain shape (i.e., stripe or polygon), and certain orientation. In addition, the boundary regions between the adjacent domains form complicated topological networks.

In any of the samples in Figure 1b–d, the interconnected boundary and domain regions may have two dual functions in altering the local shear behavior for MGs: One is to block the propagating shear band, which may be optimized if the domains or the interface boundaries are stronger and made perpendicular to the shear direction. This mechanism is known already as the guiding principle in making MG composites.[7–14] Another, less thought about, is to distribute some weak domains or boundaries such that one can deliberately guide the formation and propagation of the local deformation in specific directions and regions (see below). By doing so, one can divert and control the local shear to gain plasticity and at the same time, avoid disastrous brittle fracture caused by unmanaged shear banding. By spatially patterning the weak and strong heterogeneous domains and boundaries, therefore, we expect to let the two function synchronously so we can achieve the goal of enhancing plasticity as well as strength through optimizing the geometry and topology of the heterogeneities.

In this article, we will focus on the pattern with polycrystalline microstructures shown in Figure 1d as an example to demonstrate the ideas and reveal the underlying mechanisms

for improving plasticity and strength. We expect that the basic mechanisms discovered here should still operate for other patterns although certain variations may occur due to differences in the topology of the patterns. These results will be reported in separate publications. In the following, we aim to prove our hypothesis by using numerical modeling.

Methods

To establish the relation between the microstructure patterns and the mechanical properties in the GMGs on relatively large scales so that comparison can be made to experiment, we use a continuum approach, finite element modeling (FEM), to model the mechanical behaviors of the model GMGs. The samples consist of a number of discrete material elements, each of which is governed by the proper constitutive equations for mechanical behavior as described next. For a cubic element in three dimensions or square element in two dimensions, its side length is designated as d. The FEM can handle the length as well as time scales comparable to experiment ranging from hundreds of nanometers to microns, and nanoseconds to seconds, which is unapproachable by other modeling approaches such as molecular dynamics (MD) methods that can only deal with the sample size and the time typically within the range of tens of nanometers and nanoseconds. As discussed in the "Discussions" section, the small size not only makes it difficult to compare to experiment for such highly heterogeneous samples, but also does not warrant reliable statistics in microstructure properties, which is crucial to investigating GMGs.[20]

The microstructure pattern shown in Figure 1d is generated from the Voronoi tessellation,[27,28] or using the digitized SEM micrograph of vapor-deposited MGs.[29] Once the microstructure pattern is created, we can divide the entire sample into meshes of finite elements and associate each finite element to either a grain or a grain-boundary according to the geometric and topological properties of the underlying pattern.[30] In other words, the elements are sorted into two groups: one is tagged as grain and the other boundary.

Because the total volume of a sample is fixed, once the number of grains N is chosen, the (mean) grain size D is fixed, which is measured as the number of elements in each grain. Under the plane strain condition with a given sample area, the mean grain size D is inversely related to the number of grains N, that is,$D \propto 1/N^{1/2}$. Therefore, the larger a grain size is, the smaller the number of grains N is, and vice versa. Grain-boundary width W can be measured by the number of elements across the boundary, so W can be expressed as a multiple of d. The narrowest boundary has the width with only one element (i.e., $W=1$). In FEM, the smallest deformation unit is also the element; therefore, the local shear can be identified when the smallest unit deforms. **Figure 2** shows some typical samples with different sets of parameters in N and W.

In addition to the microstructure parameters, D or N and W, the corresponding free volume density ρ and ρ_B can be assigned to each element in the grains and on the grain boundaries. A region with a smaller free volume density is harder or stronger mechanically and vice versa.[18,30] Therefore, by distributing different ρ and ρ_B in grains and grain boundaries, we can make a GMG heterogeneous in the mechanical properties in the spatial patterns. Therefore, the local regions with varying FVs have different thermomechanical properties, which are the function of the internal variable of the FVs. In addition to the spatial distribution, there are various ways to generate free volume densities from different statistical distributions, which are known to impact the mechanical properties.[18] In this article, we will use the random distribution,[18] which is close to that in monolithic MGs made by rapid cooling in experiment.

The mechanical properties of the GMG samples are obtained by using an elastoplastic constitutive model that considers FV variation under applied stress or deformation strain.[18–20, 30–32] The deformation strain in this model consists of elastic and plastic parts, $\epsilon_{ij} = \epsilon_{ij}^{el} + \epsilon_{ij}^{pl}$, where ϵ_{ij}^{el} is the elastic strain of an isotropic sample and $d\epsilon_{ij}^{pl} = d\lambda \frac{\partial g}{\partial \sigma_{ij}}$ the plastic flow equation for the plastic potential function, $g(\sigma_{ij}) = b'I_1 + \sqrt{3J_2} - K$, λ the plastic deformation parameter related to free volume change, σ_{ij} the Cauchy stress, and I_1 the first invariant of the stress tensor σ_{ij}, and J_2 the second invariant of the deviatoric stress. The effective stress and increment of equivalent plastic strain are $\sigma_{DP} = a'I_1 + \sqrt{3J_2}$ and $d\epsilon_{eff}^{pl} = \sqrt{2/3 d\epsilon_{ij}^{pl} d\epsilon_{ij}^{pl}}$. a', b' and K are constant where $a' = b'$, or the associated flow rule, is assumed.

The plastic strain rate is related to the free volume production

$$\dot{\epsilon}_{eff}^{pl} = 2f \exp\left(-\alpha v^* / \bar{v}_f\right) \exp\left(-\frac{\Delta G^m}{k_B T}\right) \sinh\left(\frac{\tau \Omega}{2 k_B T}\right)$$

and

$$\frac{\partial \bar{v}_f}{\partial t} = v^* f \exp\left(-\alpha v^* / \bar{v}_f\right) \exp\left(-\frac{\Delta G^m}{k_B T}\right) \left[\frac{2\alpha k_B T}{\bar{v}_v S}\left(\cosh\left(\frac{\tau \Omega}{2\alpha k_B T}\right) - 1\right) - \frac{1}{n_D} + \kappa \nabla^2 \bar{v}_f\right],$$

where $\bar{v}_f$ is the mean-free volume, α a geometrical factor that is close to 1, v^* the hard-sphere volume of an atom, k_B the Boltzmann constant, Ω the atomic volume, τ the equivalent shear stress, ΔG^m the activation energy, f the frequency of atomic vibration, T temperature, n_D the number of atomic jumps needed to annihilate a free volume equaling to v^*, which ranges between 3 and 10, and $S = \frac{E}{3(1-\mu)}$, where E is the Young's modulus and μ Poisson's ratio, and κ a free volume gradient coefficient. To solve the above nonlinear equations for $\bar{v}_f$ and ϵ_{ij}, we implement the material tangent matrix $D_{ijkl}^{ep} = \partial \Delta\sigma_{ij} / \partial \Delta\epsilon_{kl}$ in ABAQUS finite element software through a UMAT subroutine. We use the properties of

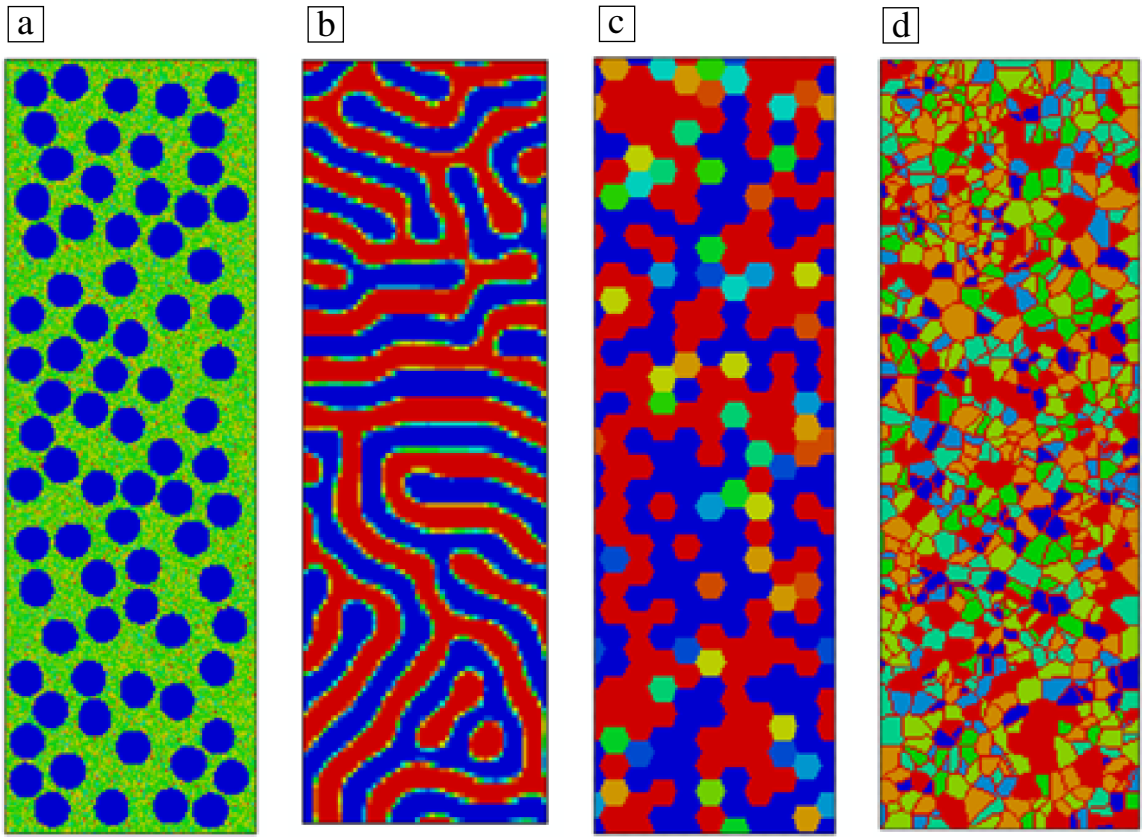

Figure 1. The patterns formed by the regions of heterogeneity in (a) the conventional metallic glass (MG) composites formed by mixing inclusions made of particles or fibers (filled blue circles) into the MG matrix, (b) by chemical spinodal decomposition which forms bicontinuous MG regions (red and blue stripes), (c) artificial honeycomb lattice (filled hexagons), and (d) the polycrystalline or granular pattern with stochastically distributed domains, or grains, and interconnected grain boundaries. Here, we use free volume density to represent heterogeneity. The different colors represent different free volume densities.

$Zr_{41.25}Ti_{13.75}Ni_{10}Cu_{12.5}Be_{22.5}$ MG, or Vitrelloy I (Vit 1), at 300 K here for our modeling.[30–32] Plane strain tension load is applied to the samples with the strain rate of 0.1/s. The samples have 30,000 regular square mesh elements with the periodic boundary conditions (PBCs) implemented.

The detailed modeling and sample parameters used in this work are briefly described here: (1) The four parameters, N or D, W, ρ and ρ_B are chosen with the following values: the mean FV density ρ for the grains is 0.05 from the monolithic MG,[18] ρ_B from 0.01 to 0.11 so we can see how the boundaries affect the overall mechanical properties with the boundary FV change from small $\rho_B(= 0.01)$, or "hard" boundaries, to larger $\rho_B(= 0.11)$, or "soft" boundaries. (2) N is chosen as 25, 50, 100, 150, and 200. (3) W is taken as 1, 2, to 3. As mentioned before, the grain size D is directly related to N. Figure 2 shows the GMG samples with $N = 50$ (a and d), 100 (b and e), and 200 (c and f) grains, and different boundary thickness $W = 1$ (a, b, and c) and 3 (d, e, f). As shown next, the choice of these parameters allows us to carry out a systematic investigation of the microstructure–property relations in the GMGs that has not been done before.

Results

Synopsis of mechanical properties of GMGs

Compared to the monolithic MGs and the random MG composites (Figure 1a), the GMG samples with polycrystal-like microstructure shown in Figure 1d are defined by a wide range of microstructural parameters (i.e., the domain or grain size, D, the boundary width between adjacent grains, W, as well as the FV densities within the grains, ρ, and on the boundaries, ρ_B). These four parameters quantify the spatially patterned FV heterogeneities. The geometric and topological structures, in addition to the FVs, are sufficiently complex to allow us to examine the general principles or mechanisms of how spatially patterned heterogeneities affect the ductility and strength of GMGs. From these results, we may get valuable insights about the structure–property relations for other patterns, including those in Figure 1b–c.

It is well known that the microstructure plays important roles in mechanical properties of polycrystals.[27] When the grain size decreases to submicron or nanometer scales, the yield strength increases via the Hall–Petch relation. Approaching below about

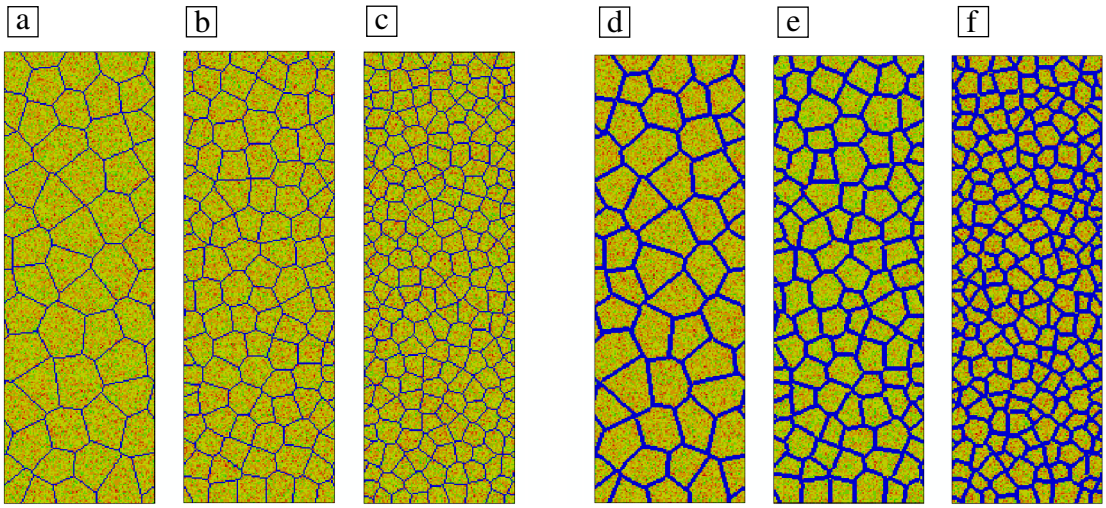

Figure 2. The spatially patterned granular metallic glass samples with $N = 50$ (a and d), 100 (b and e), and 200 (c and f) grains, and different boundary thickness $W = 1$ (a, b, and c) and 3 (d, e, f). The length scale is in the unit of d.

100 nm, the polycrystals exhibit weakening in strength, or the inverse Hall–Petch effect. In comparison, MGs do not naturally possess microstructures in rapid cooling of the liquids. As seen next, in the artificially patterned GMGs with the polycrystal microstructures, we expect to see far more complicated variations in both the plasticity and the strength as a function of these microstructure parameters.

Figure 3 shows the stress–strain curves for the GMG samples subject to tension. From these relations, we can obtain various mechanical properties with different microstructures. For comparison, we plot the stress–strain curve for the monolithic MG with a mean FV density at 0.05.[20] In all cases, we see that there is a linear elastic regime within about 1% strain followed by a nonlinear elastic regime. Following the convention, we determine the yield stress by the 0.2% offset strain method. The peak stress, the highest stress in the stress–strain curves, is at about 2% strain. After reaching the peak stress, the stress plunges and is followed by a "flow" regime with a leveled flow stress at larger deformation strain. Note that due to the PBCs used in the FEM, the samples do not fracture abruptly when the stress drop occurs. Instead, it continues to deform, which allows us to observe the formation and propagation of shear bands confined by the microstructures (see next). Therefore, we can treat the peak stress, the stress drop, and the associated sample strains as an indication of the limit of the plasticity in our analysis. With the large deformation strain passing the value corresponding to the peak stress, we can see that there emerges a second peak of stress at larger strains that resembles the "ultimate strength" during work hardening in ductile crystalline materials such as steels. This is a unique result from the GMGs. As seen next, because the change of the plasticity is also reflected in the subsequent "flow stress" after the stress drop and the rise of the second stress peak, we will also utilize this quantity as another indication for plasticity.

In polycrystalline materials, the strength as well as plasticity increase with the decreasing grain size described in the Hall–Petch relation, and at much smaller grain size in nanometer regime, softening occurs, which is described as the inverse Hall–Petch effect. The GMGs exhibit much complicated behavior. Figure 3a–c shows that the overall strength in the GMGs can either increase or decrease with the same grain size that depends sensitively on other microstructure parameters, namely, W and ρ_B. For instance, if the boundaries are harder, or have lower FV density ρ_B, the decreasing grain size induces hardening. In addition, this trend becomes more dramatic when the boundary width W is wider as shown by the thicker lines in each case with the increasing W in Figure 3a–c. In comparison, we seldom observe this phenomenon in polycrystals.

Besides the unique variation of the yield and peak stress, the flow stress after the stress drops no longer remains flat as shown in Figure 3c; it rises up at larger applied strains when N gets larger, or the grain size decreases, or the grain boundaries are wider (Figure 3b–c). The rise of the flow stress appearing at larger deformation strains signals an emergence of some kind of work hardening in the GMG with the harder boundaries. In a sharp contrast, if soft boundaries with larger ρ_B values are introduced, the strengthening and work-hardening effects diminish all together, and even worse, softening prevails. This trend becomes more pronounced when the boundary width W increases and the grain size D becomes smaller.

Microstructure–property relations

The general trend of the change of the strength and plasticity versus the variation of the four microstructure parameters can be extracted from the data in Figure 3. The results are summarized

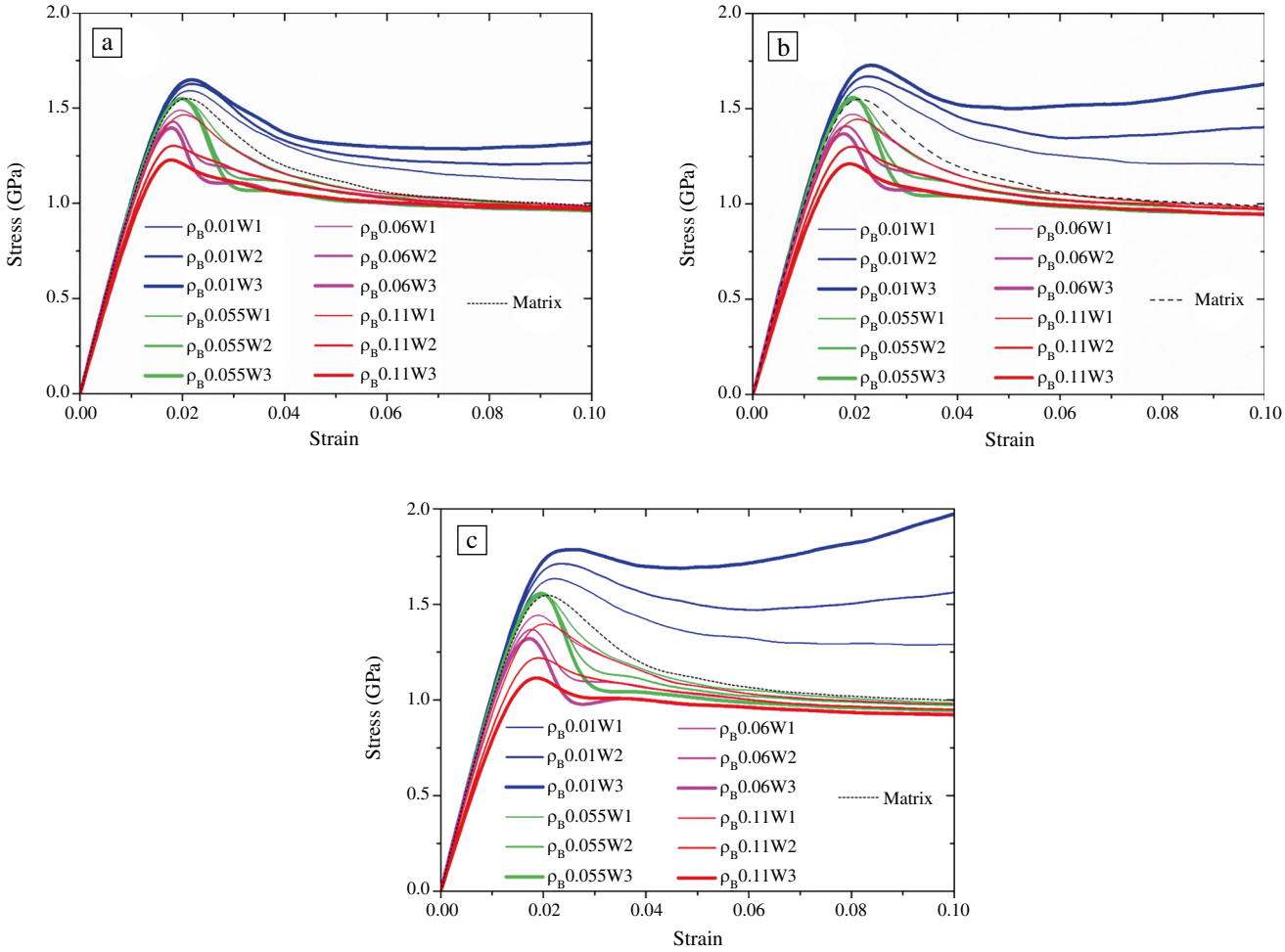

Figure 3. The tensile stress–strain relations in the patterned granular metallic glasses with free volume (FV) heterogeneities that have different numbers of grains, (a) N = 50, (b) 100, and (c) 200. In each case, the grain-boundary FV density (ρ_B) and the boundary width (*W*) are labeled in the legend. For comparison, the stress–strain relations for the monolithic MG matrix with ρ = 0.05 are plotted with a black-dashed line. In each figure, the line thickness represents the boundary width *W* and the line color denotes different boundary free volume density, or hardness/softness. Due to numerical instability at large applied deformation strains (>50%) in the finite element modeling, we only plotted the stress–strain curves up to 10% strain.

in **Figure** 4a–c for yielding stress, peak stress, and flow stress. One can see quantitatively the trend of the hardening and softening of the GMGs versus the grain size, and other microstructure parameters. And more importantly, one can see the precedence of the influence of these parameters: The most influential is the grain-boundary FV density ρ_B or the hardness or softness of the grain boundaries. It sets the trend for changing strengthening and plasticity when other parameters are introduced: Once ρ_B is set, the influence of other parameters, the grain size *D* and the grain-boundary thickness W, on the mechanical properties exhibits systematic variation.

Figure 4d shows the plastic strain versus the grain size under different ρ_B and W. Here, we measure the plasticity by the strain limit corresponding to the peak stress. In each case, one can see that for a given *N*, which is inversely related to *D*, the corresponding strain at the maximum stresses increases with the decreasing ρ_B and the increasing W, and vice versa. This trend follows exactly that of the maximum stress as seen above in Figure 4b but in the opposite trend, except for the samples with soft boundaries with larger boundary FVs: When ρ_B = 0.11, the plastic strain increases with decreasing grain size. The softening is clearly caused by the softer MG on the boundaries. In addition, the enhancement of the plasticity can also be seen in the appearance of the flow stress at larger strains in the cases shown in Figure 3b and c when the number of the grains increases. Note that we did not use the yield strain here to measure plasticity because the enhanced strength causes the increase in the Young's modulus too, which effectively lowers the yield strain by shifting the yield point to the smaller strains, or causing the yield strain to decrease.

Accompanied with the change of plasticity is the change of the toughness. By integrating the stress–strain curves in

Figure 3, we have the mechanical energy per unit volume shown in Figure 4e that is plotted against the variation of the grain diameter D under different boundary FV density ρ_B and thickness W. One can see the same trend as in the strength (Figure 4a–c) as well as plasticity (Figure 4d), that is, the improvement in the strength as well as the plasticity by patterning the FV heterogeneity can simultaneously enhance the toughness.

Underlying deformation mechanisms

The dependence of the strength, plasticity, and toughness on the grain size and other microstructure parameters in the GMGs is closely related to the underlying deformation mechanisms of local deformation (i.e., the formation and propagation of the local shear bands, which are the narrow regions with a higher local deformation strain than the rest of the samples). When the applied external stress approaches the yield stress, the regions with loosely packed atomic density, or higher FV density, start to deform more and eventually form the local shear bands. The newly formed shear bands have certain size or thickness depending on the applied stress and local confinement of the sample,[33–35] usually around tens of nanometers to microns. Upon further loading, these shear regions propagate and grow, and as a result, become larger or thicker, and eventuall become mature shear bands, which are the major strain carrier for the MGs. Some of these local shear regions can become so large locally that they eventually cause fracture. From this general mechanism, we can understand how and why patterning heterogeneity in the GMGs can be so effective to enhance the ductility, or toughness, as well as strength of MGs that are otherwise brittle macroscopically.

Figure 5 shows the contour plot of the local shear stress, strain, and the FV in the GMG samples undergoing tensile deformation at various applied strains. For clear comparison, we took the samples with the largest change in strength, plasticity, and toughness with the change of grain diameter. One is the sample with $N = 50$ grains or larger mean grain size, the widest grain boundaries width $W = 3$, and the softer boundaries with a high FV density $\rho_B = 0.11$ (Figure 5a–e). From this sample, one can see that deformation starts at the soft boundaries early on when the applied strains are even below the yield point (applied strain $\varepsilon = 0.01$ in Figure 5a1–3). The distribution of the largest local strains and stresses match exactly the pattern of the grain boundaries (Figure 5a2 and a3); the regions around the boundaries also show some deformation, albeit small. As the applied strain becomes larger, the local deformation (Figure 5a2–e2), primarily at the boundaries, becomes larger, and the FVs in the boundaries and the peripherals increase (Figure 5b1–e1). At larger applied strains ($\varepsilon > 0.03$), some local deformation diminishes and others become larger and more extended but still follow the pattern of the boundary networks. These consolidated local deformation zones eventually become (a few larger) shear bands with extended length and width ($\varepsilon = 0.05$ or Figure 5e1–2) Once the large shear bands form, the local stresses drop as a result in the corresponding locations (Figure 5e3). Due to the PBC used here, these shear bands continue deforming, which allows us to observe the entire evolution of the local deformation mechanisms.

As a contrast, the other sample has the lowest boundary FV density, $\rho_B = 0.01$, or the boundaries are harder than the interior of the grains (Figure 5f–j). As a result, it shows just the opposite trend to the previous case: The harder boundaries have higher local stress and as a result (Figure 5f3–j3), the deformation starts early on elsewhere outside of the boundaries ($\varepsilon = 0.01$ in Figure 5f2). As the applied strain increases, the softer grain interior deforms with larger deformation strains while the boundaries have smaller deformation. In the meantime, the deformation in the interior of the grains starts also showing development of a vast number of small local shear zones, which can be observed clearly as fine stripes of shear strain zones with larger FVs at the applied strain ε from 0.01 to 0.03 (Figure 5f1–i1 and Figure 5f2–i2). At higher strain ($\varepsilon \geq 0.03$), one can see from Figure 5j that some shear zones evolve into large shear bands, and at the same time, many subbands with smaller sizes emerge also. The larger shear bands are also fragmented as they are cut or blocked by the harder boundaries (Figure 5f1–i1 and f2–i2), while the smaller subbands, mostly still made of smaller deformation zones, are confined inside the grains. At all deformation stages, the local stresses at the boundaries remain higher than these inside the grains (Figure 5f3–i3). Compared to the softer boundary case (Figure 5a–e), the local stress distribution, instead of local strains, remains high in value throughout the deformation process in the boundary regions and maintains the same pattern conforming to that of the grain-boundary networks (Figure 5 i–j).

Discussions

Redistribution of local stress and strain by spatial patterning heterogeneities

The detailed mapping of local stress, strain, and free volume change in the GMGs during deformation reveals the deformation mechanisms underlying the observed change in the strength, plasticity, and toughness. As previously mentioned, the dislocation-based strengthening mechanism in crystals is primarily through dislocation interactions with each other and with other microstructure entities such as grain boundaries and precipitates. The deformation induced by shear localization in MGs is a softening phenomenon by nature. The local deformation or shear alters the atomic packing by introducing more FVs, and these regions become softer in subsequent deformation that leads to larger shear bands and consequently catastrophic failure. Obviously, one cannot follow the example in crystalline materials by simply creating more shear bands to strengthen and toughen the MGs.

However, through artificial patterning, we show that we can redesign and reengineer the local shear in the MGs to improve the mechanical performance of this class of metallic

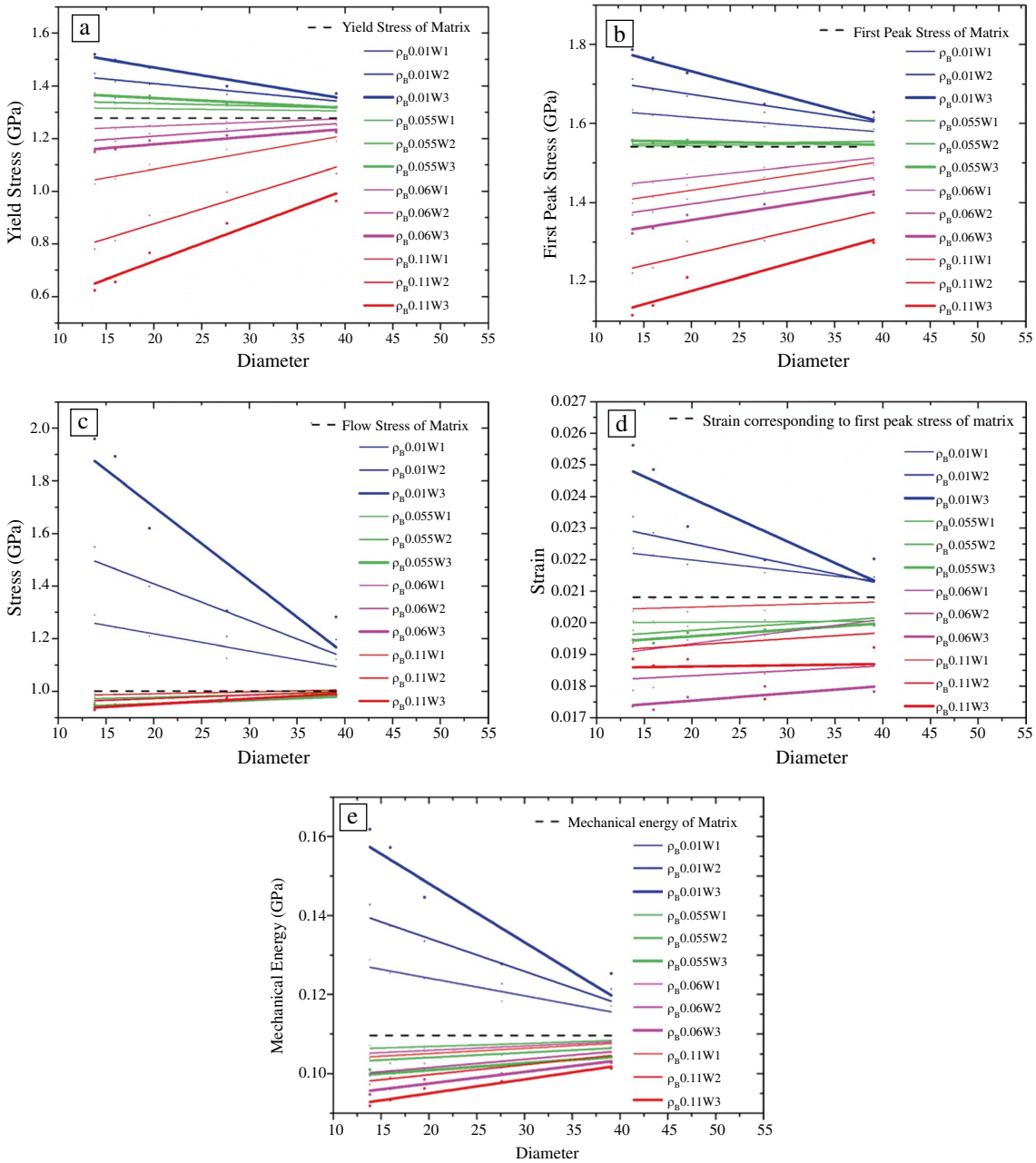

Figure 4. The characteristic mechanical properties exacted from the stress–strain curves in Figure 3 versus the grain size *D* or the numbers of grains *N*: (a) yield stress, (b) the first peak stress, (c) flow stress, (d) the strain corresponding to the first peak stress, and (e) the mechanical energy, or toughness represented by the integral over the stress–strain curves. In each case, the grain-boundary free volume density (ρ_B) and the boundary width (*W*) are also labeled in the legend. The lines linking the finite element modeling datum points are the guide to the eyes.

materials. Specifically, we learned that we can manipulate the local shear through introducing the boundaries. One way is to change the boundary FV density and the other the width, which as we show below, is closely related to the grain size also. The boundary FV density allows for redistribution of local strains in the softer boundaries and local stresses in the harder boundaries. The spatial patterning of FVs is essentially patterning the local stress and strain states that can set a new local deformation condition for selectively altering the shear deformation behavior.

For the soft boundary case, shear initiates at the boundary first and can become more pronounced there. Therefore, the granular pattern allows for control of the deformation zones that form and move in specific locations. For the hard boundary case, shear

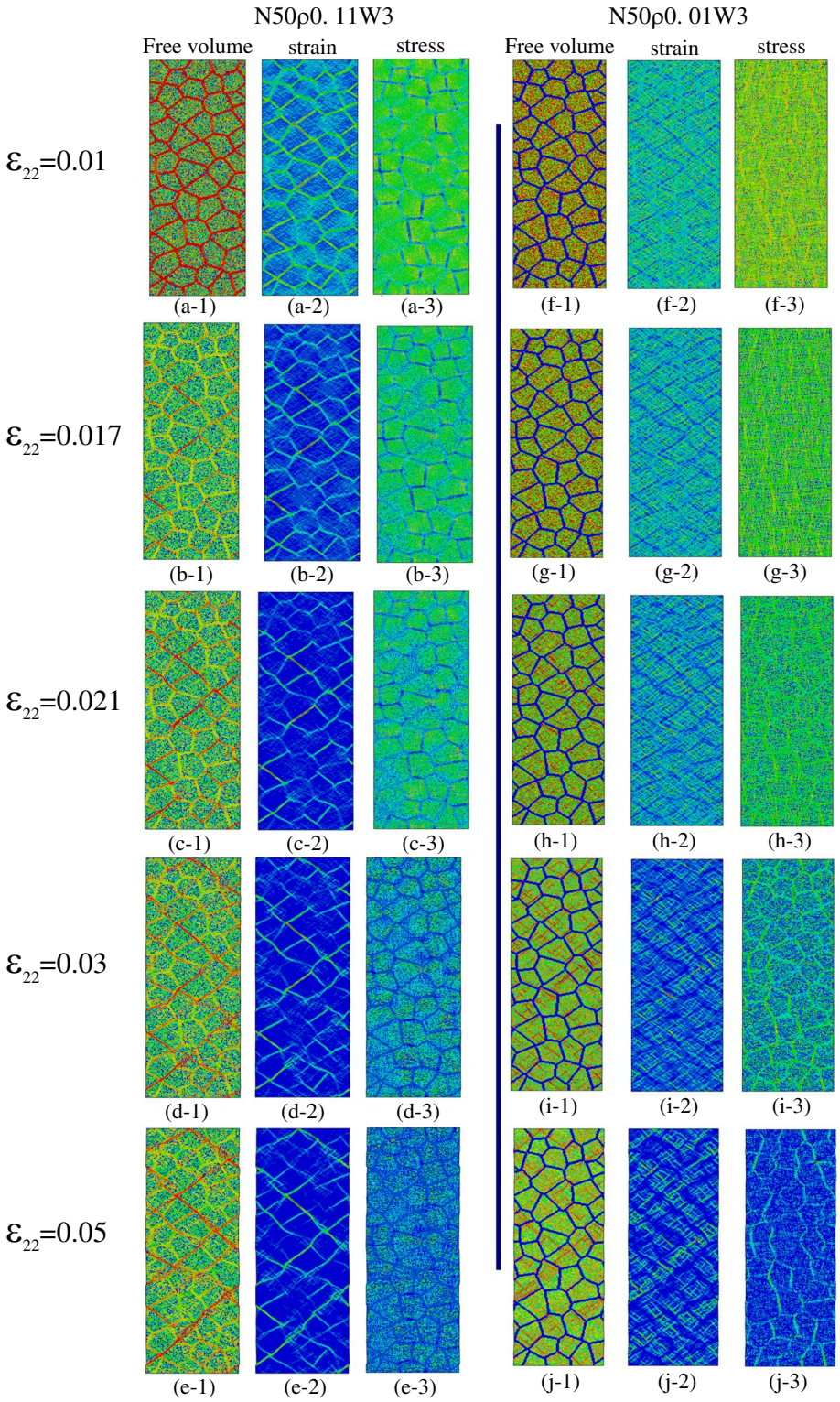

Figure 5. The contour maps for local free volume, stress, and strain in the sample undergoing deformation at various strains. The samples with $N = 50$ and $W = 3$ are taken as the two extreme cases with $\rho_B = 0.11$ (left) and 0.01 (right). The color scheme is such that the lighter or warmer the color is, the higher the amplitude of the corresponding quantity it represents.

deformation initiates inside the grains, and once formed, is localized and confined inside also. The boundaries not only partition the deformation zones, but also block the propagating shear zones or bands once formed inside the grains. Therefore, this sets an optimal condition to achieve both plasticity by initiating large shear deformation inside the grains and enhancing the strength by limiting its spreading and forming of large and penetrating shear bands. In other words, the massive number of local shear zones and bands inside the grains contributes to the enhancement of plasticity; and at the same time, it is difficult for these small shear bands to merge into supersized ones that then propagate across the hard boundaries and the entire sample to cause failure is the origin for the increase in the strength.

Effects of microstructures

As compared to polycrystals, a GMG can achieve both strengthening and softening with a given grain size. This particular property is connected to the unique deformation mechanisms discussed above as well as the multiple microstructure parameters in the GMGs that one can control simultaneously. For instance, once the boundary FV density is given, the trend of the dependence of the strength and plasticity on grain size is determined: The harder boundaries always induce hardening and ductility, whereas the soft ones can lead to plasticity, either softening or strengthening, and brittleness as well.

On the other hand, changing the boundary width W affects the mechanical properties through two routes. One is the minimum shear band size. In monolithic MGs, when the yield point is approached, many small local

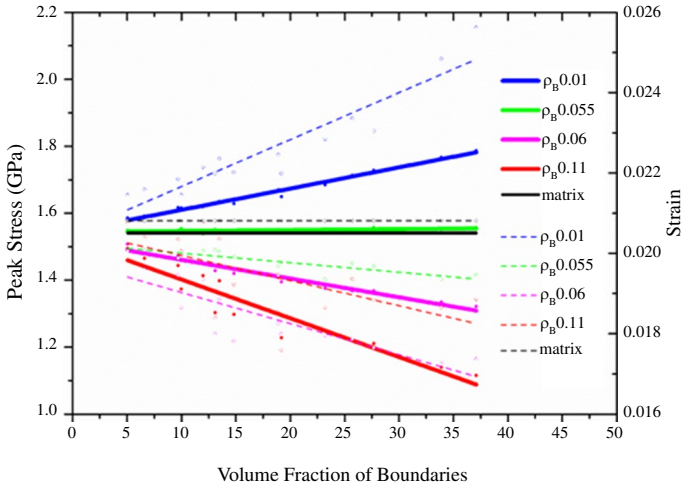

Figure 6. The peak stress (solid lines) and strain (dashed lines) versus the volume fraction of the boundaries in all samples we used here with different numbers of grains and boundary width. Different colors represent different boundary-free volume densities. The lines are drawn to guide the eyes.

shear zones form in the regions with high FV densities. As applied strain increases, these small deformation zones eventually grow and consolidate to form large stripe-like bands (Figure 5) with the minimum thickness of about tens of nanometers to submicrons. When this happens, the bands propagate and broaden at the same time. If not stopped or diverted, these large softer banding regions become the major deformation strain carrier and cut through the sample, leading to fracture or brittleness. In GMGs, shear zones also form in the softer regions, either inside the grains if the boundaries are harder, or in the boundaries if the grain boundaries are softer. In the latter, if the grain boundaries are narrower than the minimum shear band size, shear banding would be difficult to form in the boundary regions even when it is softer. In our FEM, the minimum size that allows for local shear is the finite element size d. For the boundaries with the grain-boundary width smaller than or equal to this size, or $W \leq d$, shear band formation is either difficult to happen or delayed to larger applied strains. However, when $W > d$, shear band formation is relatively easier on the boundaries (Figure 5). This size dominated selective deformation on the softer boundaries is vividly captured in the FEM model for the case with $\rho_B = 0.11$ and different width Ws (Figures 3, 4, 5): The samples with the wider boundaries become softened easily and the deformation occurs with high probability in the softer and wider boundary regions.

For the cases with harder boundaries, the shear zones occur inside the softer grains. Because our samples have grains always larger than the minimum shear band size, one can see that the shear deformation zones emerge inside the grains relatively easily (Figure 5), and these zones eventually form larger shear bands also inside the grains. One can imagine though that when the grain size D is smaller than or equal to d, the local shear inside the grains would become difficult; even when the grains are softer.

Changing the boundary width W and the number of grains N amounts to changing the volume of the boundaries because the boundary volume is the product of the boundary area and the width. In other words, patterning the heterogeneity through variation of the microstructure parameters is equivalent effectively to making a MG composite albeit with precise control of the grain boundaries as the inclusion and the grains as matrix. The overall mechanical response is, therefore, the weighted contribution from the boundaries and the grains. For all cases shown in this work, the corresponding volume fraction of the boundaries for W = 1, 2, and 3 is 5.06%, 9.99%, and 14.8% for N = 25, 6.6%, 13.1%, and 19.2% for N = 50, 9.7%, 18.9%, and 27.7% for N = 100, 12.0%, 23.2%, and 33.9% for N = 150, and 13.5%, 25.9%, and 37.1% for N = 200, respectively. **Figure 6** illustrates the strength and plasticity change versus the volume fractions for the GMGs with different boundary FV densities. One can see that when the boundaries are harder with smaller ρ_B, the strength shows an increasing trend with increasing volume fraction of the harder boundary phase; as ρ_B gets larger for the softer boundaries, the trend goes down, or the GMG becomes softer. The same is found for the plastic strains.

From GMG to nanoglass: The challenge in overcoming size and time limitation

The FEM used in this work has the length scale on the order of submicron as determined by the gradient term and the material propertied in the constitutive model. The shear bands formed in the modeling are roughly tens of hundreds of nanometers or submicron in thickness (Figure 5), which is in line with the experimentally observed shear band size. In other words, our work provides the structure–property relations for the GMGs with the grain size on the micron scale. When the grain size reaches nanometer scale (<100 nm), the GMGs are called NG.[22] Extensive work has been done in the past that show some new and improved mechanical properties in the NGs.[36–46] Atomistic simulation, in particular molecular dynamics simulation, has been extensively performed to investigate deformation mechanisms and the effects of the microstructures.[47–57] However, the sample size and also time duration in MD simulation are limited to about less than 10 nm and tens of nanoseconds in most cases. In other words, the typical grain size is about 8 nm, usually about less than 100 grains are handled in the NG samples.[47–57] In addition, due to the time limitation, the strain rate in a typical MD simulation is in the range between 10^9 or 10^{10} 1/s, whereas the experimental strain rate is usually orders of magnitude smaller. Because the typical thickness of the shear bands observed experimentally is about tens of nanometers to submicrons and the applied strain rate is around 10^{-4} 1/s, the shear deformation process obtained

in the MD modeling can only be considered as specific cases under these extreme conditions.

Small sample size can also pose other challenges, one of which is statistical reliability for heterogeneous systems. The limited number of grains used in modeling is known to produce poor statistics in acquisition of the structure–property relation. One of the consequences is the strong artificial dependence on grain-boundary orientation: In a sample with a total of about a few tens of grains, the number of grains across the sample is about five or less. If one or two grain boundaries between these grains are oriented along the approximate direction of the MRSS, in the event that a large shear band could initiate in the boundary, it can traverse the sample easily, causing brittle failure. This outcome is not intrinsic of the NGs but the limited sample size, or the limited number of grains. As we have shown here in the FEM, in a sample with a sufficiently large number of grains, the local deformation can be contained by the surrounding grains and grain boundaries.

On the other hand, although the FEM does not suffer from the same limitations unique for atomistic modeling, more detailed information is needed from the nanoscales in order to extend the FEM to modeling the NGs. This requires us to acquire some necessary length-related properties such as free volume gradients or thermal gradients, detailed interface properties, and thermomechanical properties in the NGs during deformation so we can calibrate the constitutive model. Unfortunately, these essential parameters are not available yet. But with the progress in NG research, especially nanoscale probes, we expect a fully functional FEM model for NGs.

Conclusions

Monolithic metallic glass is a quasi-brittle material marked by the lack of macroscopic plasticity. This shortcoming is the major factor limiting the application of this class of metallic materials. In this article, we examined a new way to enhance its plasticity via patterning the amorphous phases into granular patterns with harder or softer grain or boundary regions. By introducing the microstructures in the structureless MG, we gain a larger parameter space that enables us to manipulate and control the local shear deformation behavior. Using FEM, we demonstrate that the mechanical properties of the MGs can be redesigned and reengineered effectively by simply dressing the boundaries with either harder or softer MGs or other phases with different (micro)structures. Desired plasticity and strength can be achieved by tuning the microstructure parameters.

It is well known that polycrystalline materials can be engineered to achieve remarkable properties with the naturally present microstructures, including the nanocrystalline materials.[22,27] Introducing microstructures to form the granular MG is a new concept. This article shows the possibility to change the mechanical properties of MGs with out-of-the-box thinking if the artificial microstructures are properly introduced and engineered. Our work provides the first systematic investigation of how the four essential microstructure parameters contribute quantitatively to the mechanical properties of the GMGs.

Recent experimental work in synthesis of nanoglass from the nanosized MG particles or domains formed during evaporation and condensation in IGC or vapor deposition provides support for this idea. By compacting the loose nanosized powders, bulk NGs with grain boundaries can be produced. A similar approach has already been successfully applied in making nanocrystalline materials.[22] The granular NGs exhibit some remarkable changes in their physical and mechanical properties.[1,36] Nevertheless, there are still many profound differences between the general GMG on micron or larger scales and the NG, especially for numerical modeling. Although the atomistic modeling on the nanoscale and nanosecond scale needs to extend to larger spatial and time scales, the FEM could benefit the detailed atomic mechanisms in building constitutive relations that can handle deformation in smaller scales.

The mechanisms and relations between the microstructure and properties revealed in this work may help us to understand other types of GMGs (Figure 1). These patterned microstructures can be made either stochastic like the granular MGs or more regular through 3D printing.[37] The boundaries can be made with more controlled geometry and microstructure properties, although making nanoscale microstructure remains a challenge. No matter what processing path we choose, we need to know more about the fundamental mechanisms and microstructure contributions to the structure–property relations for the GMGs for effective engineering and application of this remarkable class of materials. We hope that our work would stimulate more interests along this direction.

Funding

Y.W.W. is supported by the Fundamental Research Funds for the Central Universities (FRF-TP-20-028A1) and the Fundamental Research Funds for the Central Universities and The Youth Teacher International Exchange & Growth Program (QNXM20210044).

Data availability

Data used in this work are available from the authors upon request.

Code availability

The code used in this work is primarily from ABAQUS, which is available commercially.

Conflit of interest

Here, we declare there are no financial and personal relationships with other people or organizations that could inappropriately influence (bias) this work.

References

1. L.G. Sun, G. Wu, Q. Wang, J. Lu, *Mater. Today* **38**, 114 (2020)
2. C.A. Schuh, T.C. Hufnagel, U. Ramamurty, *Acta Mater.* **55**, 4067 (2007)
3. J.W. Liu, Q.P. Cao, L.Y. Chen, X.D. Wang, J.Z. Jiang, *Acta Mater.* **58**, 4827 (2010)
4. W.-H. Wang, C. Dong, C. Shek, *Mater. Sci. Eng. R.* **44**, 45 (2004)
5. M.H. Lee, K.S. Lee, J. Das, *Scr. Mater.* **62**, 678 (2010)

6. Y. Zhang, W.H. Wang, A.L. Greer, *Nat. Mater.* **5**, 857 (2006)
7. C. Suryanarayana, A. Inoue, *Bulk Metallic Glasses* (CRC Press, New York, 2011)
8. J. Das, M.B. Tang, W.H. Wang, J. Eckert, *Phys. Rev. Lett.* **94**, 205501 (2005)
9. K.F. Yao, F. Ruan, Y.Q. Yang, N. Chen, *Appl. Phys. Lett.* **88**, 122106 (2006)
10. S. Scudino, B. Jerliu, S. Pauly, *Scr. Mater.* **65**, 815 (2011)
11. H. Choi-Yim, W.L. Johnson, *Appl. Phys. Lett.* **71**(26), 3808 (1997)
12. C.C. Hays, C.P. Kim, W.L. Johnson, *Phys. Rev. Lett.* **13**(84), 2901 (2000)
13. D.C. Hofmann, J.Y. Suh, A. Wiest, *Nature* **451**, 1085 (2008)
14. S.F. Guo, L. Liu, N. Li, Y. Li, *Scr. Mater.* **62**, 329 (2010)
15. D.H. Kim, W.T. Kim, E.S. Park, N. Mattern, J. Eckert, *Prog. Mater. Sci.* **58**(8), 1103 (2013)
16. E.S. Park, D.H. Kim, *Acta Mater.* **54**, 2597 (2006)
17. E.S. Park, J.S. Kyeong, D.H. Kim, *Scr. Mater.* **57**, 49 (2007)
18. M. Zhao, M. Li, *Metals* **2**, 488 (2012)
19. Y.W. Wang, M. Li, J.W. Xu, *Scr. Mater.* **113**, 10 (2016)
20. Y.W. Wang, M. Li, J.W. Xu, *Scr. Mater.* **135**, 41 (2017)
21. Y.W. Wang, M. Li, J.W. Xu, *Scr. Mater.* **130**, 12 (2017)
22. H. Gleiter, *Acta Mater.* **48**(1), 1 (2000)
23. H. Gleiter, *Acta Mater.* **56**, 5875 (2008)
24. H. Gleiter, *Beilstein J. Nanotechnol.* **4**, 517 (2013)
25. J.X. Fang, U. Vainio, W. Puff, *Nano Lett.* **12**, 458 (2012)
26. C. Guo, B. Wu, S. Lan, G. Peng, X. Wang, H. Hahn, H. Gleiter, T. Feng, *Mater. Res. Lett.* **5**, 293 (2017)
27. H. Gleiter, *Prog. Mater. Sci.* **33**, 223 (1989)
28. N. Chen, D.V.L. Luzgin, K.F. Yao, *J. Alloys Compd.* **707**, 371 (2017)
29. H. Gleiter, Th. Schimmel, H. Hahn, *Nano Today* **9**(1), 17 (2014)
30. M. Zhao, M. Li, *Appl. Phys. Lett.* **93**, 241906 (2008)
31. Y.F. Gao, *Model. Simul. Mater. Sci. Eng.* **14**, 1329 (2006)
32. M. Zhao, M. Li, Y.F. Zheng, *Philos. Mag. Lett.* **91**(11), 705 (2011)
33. J. Yi, W.H. Wang, J.J. Lewandowski, *Acta Mater.* **87**(1), 1 (2015)
34. Q.K. Li, M. Li, *Appl. Phys. Lett.* **88**, 241903 (2006)
35. C.Q. Chen, Y.T. Pei, O. Kuzmin, Z.F. Zhang, E. Ma, J.T.M. De Hosson, *Phys. Rev. B.* **83**, 180201 (2011)
36. X. Wang, F. Jiang, H. Hahn, J. Li, H. Glitter, J. Sunna, J. Fang, *Scr. Mater.* **98**, 40 (2015)
37. J.J. Marattukalama, V. Pacheco, D. Karlsson, L. Riekehr, J. Lindwall, F. Forsberg, U. Jansson, M. Sahlberg, B. Hjörvarsson, *Addit. Manuf.* **33**, 101124 (2020)
38. Y. Ivanisenko, C. Kübel, S.H. Nandam, C. Wang, X. Mu, O. Adjaoud, K. Albe, H. Hahn, *Adv. Eng. Mater.* **20**, 1800404 (2018)
39. S.H. Nandam, Y. Ivanisenko, R. Schwaiger, Z. Sniadecki, X. Mu, D. Wang, R. Chellali, T. Boll, A. Kilmametov, T. Bergfeldt, H. Gleiter, H. Hahn, *Acta Mater.* **136**, 181 (2017)
40. W. Liu, B.A. Sun, H. Gleiter, S. Lan, Y. Tong, X. Wang, H. Hahn, Y. Yang, J. Kai, C.T. Liu, *Nano Lett.* **18**, 4188 (2018)
41. X. Wang, F. Jiang, H. Hahn, J. Li, H. Gleiter, J. Sun, J. Fang, *Scr. Mater.* **116**, 95 (2016)
42. S.H. Nandam, O. Adjaoud, R. Schwaiger, Y. Mohammed, R. Chellali, D. Wang, K. Albe, H. Hahn, *Acta Mater.* **193**, 252 (2020)
43. A. Sharma, S.H. Nandam, H.T. Hahn, K.E. Prasad, *Front. Mater.* **8**, 676764 (2021)
44. M. Ghidelliab, A. Orekhovcde, A. LiBassia, G. Terraneof, P. Djemiab, G. Abadiasg, M. Norddeh, A. Béchéde, N. Gauquelinde, J. Verbeeckde, J.-P. Raskini, D. Schryversde, T. Pardoenc, H. Idriss, *Acta Mater.* **213**, 116955 (2021)
45. A. Sharma, S.H. Nandam, H. Hahn, K.E. Prasad, *Scr. Mater.* **191**, 17 (2021)
46. S. Adibi, P.S. Branicio, R. Ballarini, *RSC Adv.* **6**, 13548 (2016)
47. K. Albe, Y. Ritter, D. Sopu, *Mech. Mater.* **67**, 94 (2013)
48. D. Şopu, K. Albe, *J. Nanotechnol.* **6**, 537 (2015)
49. O. Adjaoud, K. Albe, *Acta Mater.* **145**, 322 (2018)
50. C. Kalcher, O. Adjaoud, J. Rohrer, A. Stukowski, K. Albe, *Scr. Mater.* **141**, 115 (2017)
51. X. Zhou, C. Chen, *Int. J. Plast.* **80**, 75 (2016)
52. Z. Sha, P.S. Branicio, H.P. Lee, T.E. Tay, *Int. J. Plast.* **90**, 231 (2017)
53. Z.D. Sha, P.S. Branicio, Q.X. Pei, Z.S. Liu, H.P. Lee, T.E. Tay, T.J. Wang, *Nanoscale* **7**, 17404 (2015)
54. Y. Ritter, D. Sopu, H. Gleiter, K. Albe, *Acta Mater.* **59**, 6588 (2011)
55. D. Şopu, C. Soyarslan, B. Sarac, S. Bargmann, M. Stoica, J. Eckert, *Acta Mater.* **106**, 199 (2016)
56. O. Adjaoud, K. Albe, *Acta Mater.* **15**, 393 (2019)
57. S. Yuan, P.S. Branicio, *Int. J. Plast.* **134**, 102845 (2020)